The Channel for Detecting Contrast Modulation also responds to Density Modulation (or Vice Versa)

Michael J. Morgan[1]

Donald I. A. MacLeod[2]

Joshua A. Solomon[1]

[1] Division of Optometry, School of Health Sciences, City, University of London

[2] Department of Psychology, University of California at San Diego

Corresponding Author: michaelmorgan9331@gmail.com

Abstract

In textures composed of black and white dots, we modulated dot density and/or dot contrast in one direction of visual space. Just as Mulligan and MacLeod (1988) found a strong reciprocity between density and luminance for dots viewed against a darker background, we found a strong reciprocity between density and contrast: detection thresholds for in-phase modulations of density and contrast were 30% - 55% lower than detection thresholds for density and contrast modulations that were 180° out of phase. These findings support the existence of at least one psychophysical channel that is excited by both density modulations and contrast modulations. A good, quantitative fit to our data can be obtained with a two-channel model.

Introduction

Mulligan and MacLeod (1988) demonstrated what they described as a reciprocity between luminance and dot density in the perception of brightness. An otherwise-regular grid of identical white dots appeared brighter in regions where the spacing between dots was reduced. This illusory brightness difference could be cancelled by a luminance modulation (Fig. 1). Once this was done the thresholds for detecting any kind of modulation in the pattern were raised compared to thresholds for detecting uncompensated density modulations. Mulligan and MacLeod concluded that dot brightness is determined on the basis of the space-averaged luminance within a circular area a substantial fraction of 1 deg in diameter.
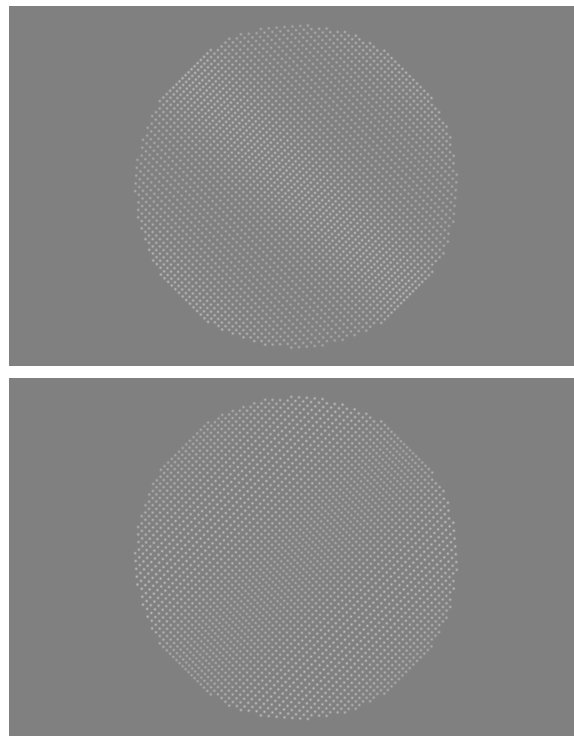

Fig. 1. In the top figure, the spacing between dots is modulated by a 45 deg sinusoidal grating in phase with their brightness (i.e., more closely spaced dots have greater intensity). In the bottom figure the two kinds of modulation are in antiphase.

On the other hand, visual estimates of average luminance may not be independent of local contrast. Indeed, in some circumstances (e.g., Solomon & Tyler, 2018) estimates

of average brightness, average darkness, and average contrast all vary with the square of local image contrast, i.e., contrast energy. Contrast-energy mechanisms have been implicated in a wide variety of visual tasks. For example, Watson and Ahumada (2011) argued that both contrast discrimination and blur discrimination were consistent with the same visual signal, a single metric of contrast energy. Morgan, Raphael, Tibber, and Dakin (2014) suggested that detection of differences in dot numerosity and dot density could also be mediated by a common contrast-energy mechanism.

A necessary step towards this synthesis is to show that Mulligan and MacLeod's reciprocity result applies to differences in contrast as well as luminance. This can be tested by composing the pattern of equal numbers of black and white dots, against a mean-luminance background, so that there is no Fourier fundamental corresponding to any modulation in dot density or contrast (Fig. 2). Using these patterns, we sought evidence for reciprocity between contrast and dot density, by measuring the threshold modulation amplitude for detecting contrast in the presence of density modulation, and vice versa. The two kinds of modulation, contrast and density, could either be in-phase, in the sense that peaks of contrast coincided spatially with peaks in density, or 180° out of phase (peaks in one domain coincided with troughs in the other). The method is similar to that by which Saarela and Landy (2012) investigated reciprocity between colour and texture in detection of an oriented edge. Like Saarela and Landy, we combined cues in roughly equivalent units of their detectability having first determined these values from trials in which only one kind of modulation was present. The method of opposition was also used by Raphael & Morgan (2016) to show that differences in dot density between two patterns are harder to detect when they are opposed by changes in pattern area that kept dot number, and hence total energy, constant.
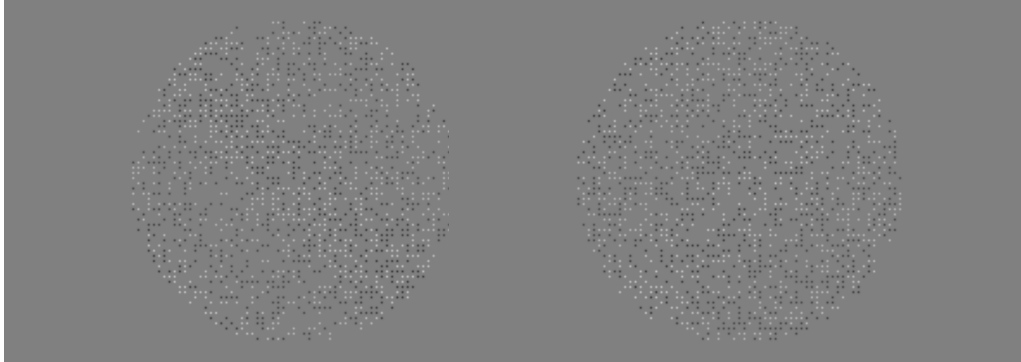
Fig. 2. Examples of stimuli combining low contrast (near threshold) density and contrast modulations in phase (left) and in antiphase (right) The basic texture in both cases consists of dots plotted at the nodes of a (notional) rectangular grid. White and black dots were plotted with equal probability, with replacement. The probability that a node is occupied is modulated sinusoidally in one spatial dimension to produce a modulation in dot density. Alternatively, or in addition, contrast is modulated at the same orientation and spatial frequency. The two kinds of modulation may be combined, either in phase or 180° out of phase, to examine possible reciprocities between them.

Methods

Participants. The participants were a 72-year-old male author (MM), a female PhD student experienced in visual psychophysics (NN), and two naïve students in their 20s from the University of Cologne subject pool (LR and SR). The use of human subjects for a non-invasive study was approved by the relevant Ethics Committee of the University of Cologne

Stimuli: Stimulus presentation was controlled by MATLAB, the PTB3 version of the Psychtoolbox (Kleiner, et al., 2007), and the Cambridge Research Systems BITS++ box to give an accurately calibrated contrast signal from a pre-computed linear look-

up table. Stimuli were presented on a Viewsonic PF817 CRT display, with pixel resolution 1024 x 768, a refresh rate 140 Hz and mean luminance 33.5 cd/m^2, viewed at 114 cm so 1pix=1.10 arcmin. Stimuli were viewed binocularly through natural pupils with appropriate corrective lenses for each subject (if normally worn). Observations were carried out in a darkened room where the only source of light apart from the display screen consisted of reflections from the matte walls and furniture.

Example stimuli are shown in Fig. 2. Each stimulus consisted of a texture of spaced dots. Each dot had a 2-D Gaussian profile with standard deviation of 2.20 arcmin (2 pix). The dots comprising the texture were presented on a notional rectangular grid of 70 x 70 dot positions with 10-pixel separation; this grid was then masked down by a circular aperture of diameter 13.6 deg, thus allowing a maximum of 70 dots along the diameter of the aperture.

To simplify calculations and notation, density and contrast modulations were initially carried out in the horizontal dimension x, producing vertically oriented textures. Density was modulated by manipulating the probability of plotting a dot as a function of grid position. We denote the probability of a dot as $p(x)$ and its peak Weber contrast as $c(x)$. The spatial frequency of modulation f was chosen to produce two compete cycles across the stimulus, and the unsigned modulation amplitudes for density and contrast are denoted m_d and m_c, respectively. In the absence of modulation (i.e., when $m_d = m_c = 0$), both the probability of a dot in any position and the absolute value of its Weber contrast were fixed at 0.5. Thus, dot probability is given by

$$p(x) = 0.5 \pm m_d \cos(2\pi f x) \tag{1}$$

and dot contrast is given by

$$c(x) = \pm \left[0.5 \pm m_c \cos(2\pi f x) \right]. \tag{2}$$

Each dot's polarity (i.e., the sign of its contrast c) was selected independently, with even odds for black and white. Modulation phases were also selected randomly, such that either the peak or the trough could appear in the centre of the stimulus. (In Experiment 2, additional constraints were imposed on modulation phases.) Finally, the entire texture was rotated around its centre by ±45 deg.

Procedure: In both experiments observers were forced to choose between positively and negatively rotated textures. Modulation amplitude was varied by an adaptive procedure to find threshold, defined as the standard deviation of the Gaussian psychometric function mapping the product of modulation amplitude (0-1) and sign (-1, +1) of rotation to the probability of reporting a positive rotation.

Experiment 1

In this experiment we wanted to establish the detection thresholds for density and contrast modulations, when observers are uncertain which dimension is being modulated. The observer initiated each trial by pressing one of the response buttons. This was followed, after a brief delay, by the stimulus presentation. The stimulus was presented for 0.5 sec, and the observer had to decide whether the texture was tilted 'left' or 'right' (i.e., positively or negatively rotated by 45 deg). The sign and absolute magnitude of the modulation amplitude on each trial was chosen on the basis of previous responses by the observer by an Adaptive Probit Estimation (APE; Watt & Andrews, 1981) designed to place stimulus values near the stationary points in the second derivative of the psychometric function (the 16% and 84% points). Trials were presented in 128-trial blocks. Density modulations (i.e., where $m_d > 0, m_c = 0$) were randomly interleaved with contrast modulations (i.e., where $m_d = 0, m_c > 0$), with no cue to the subject other than the stimulus itself to indicate which was in effect. Note that the two APE procedures were entirely separate and independent. This has the advantage that after a few trials, the two tasks (density and contrast) are equally difficult. There was no feedback.

Between 6 and 8 blocks were run on each observer. MATLAB's 'fminsearch' was used to determine the mean (the "clockwise" bias) and standard deviation of the Normal distribution that maximum-likelihood fit each set of psychometric data (i.e., one set for density modulations and one set for contrast modulations; see Fig. 3). Note that these standard deviations are reciprocally related to the observer's sensitivity.

Thus, they may be considered the detection thresholds for density and contrast modulations.[1]
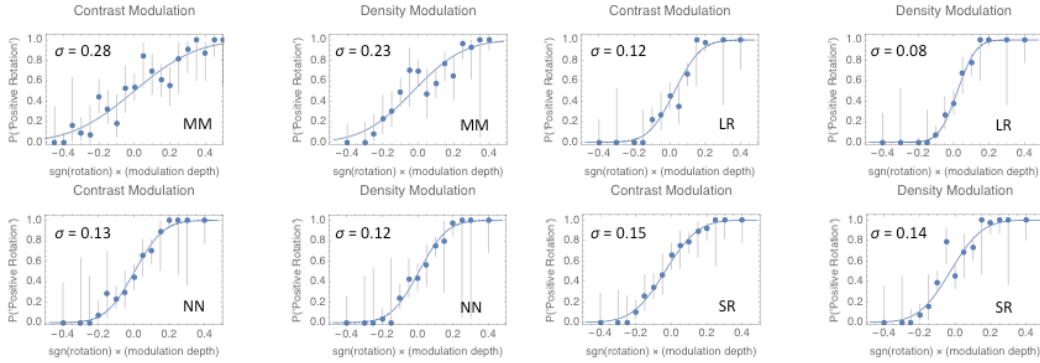

Fig. 3. Results of Experiment 1: psychometric functions for detecting contrast modulations and density modulations. Each point represents the frequency with which the observer reported a positive rotation (as in Fig. 2). Error bars contain 95% binomial confidence intervals for the response probabilities. Smooth curves are the maximum-likelihood fitting Gaussian distributions. In all cases, these distributions had inflection points near zero. Their standard deviations were considered to be detection thresholds.

Experiment 2

In these summation experiments, each stimulus contained both a density modulation and a contrast modulation, each of which was presented at the same multiple (between 0 and 3) of threshold modulation amplitude. We investigated whether in-phase modulations (i.e., where density and contrast increase and decrease together) would be easier to detect than out-of-phase modulations. As in the first experiment the observer had to decide whether the texture was tilted 'left' or 'right' (i.e., positively or negatively rotated by 45 deg). Two kinds of trial were randomly interleaved. An effect of phase angle would implicate a visual channel sensitive to modulations of both density and contrast, for instance a channel responsive to contrast energy.

RESULTS

---

[1] When replotted as percentage correct vs. log modulation amplitude, these Normal fits are too shallow. Weibull fits (Eqn. 3) are more versatile. See Supplementary Figure S1 for a graphical comparison.

Fits to the results, along with the results themselves, from each individual observer can be found in the Supplementary Material. For illustration in Fig. 4, we have summarised the fits and the results using ratios of the detection threshold. Although similar to the thresholds described in Fig. 3, these thresholds were estimated independently as the Weibull scale parameter (λ) giving a maximum likelihood it to each individual observer's responses:

$$P(\text{Correct}) = 1 - \frac{1}{2}\exp\left[-\left(m/\lambda\right)^{k}\right] , \tag{3}$$

where m represents the modulation amplitude of one component (i.e., $m \in \{m_c, m_d\}$). Functions of this form have proven to be adequate summaries of psychometric data collected using the method of constant stimuli (e.g., Watson, 1979). Consequently, we consider their fit a more reasonable baseline with which to compare more-theoretically based models than the observed $P(\text{Correct})$ itself, which often is non-monotonic when adaptive methods like APE are used. As should be clear from Eqn. 3, threshold performance is attained when $m = \lambda$, and thus $P(\text{Correct}) = 0.816$. An unbiased observer [for whom $P(\text{Correct})$ increases with all modulation amplitudes] will attain this same level of performance when $m = \sigma/1.11$. Parameter values and log likelihoods appear in Table 1.
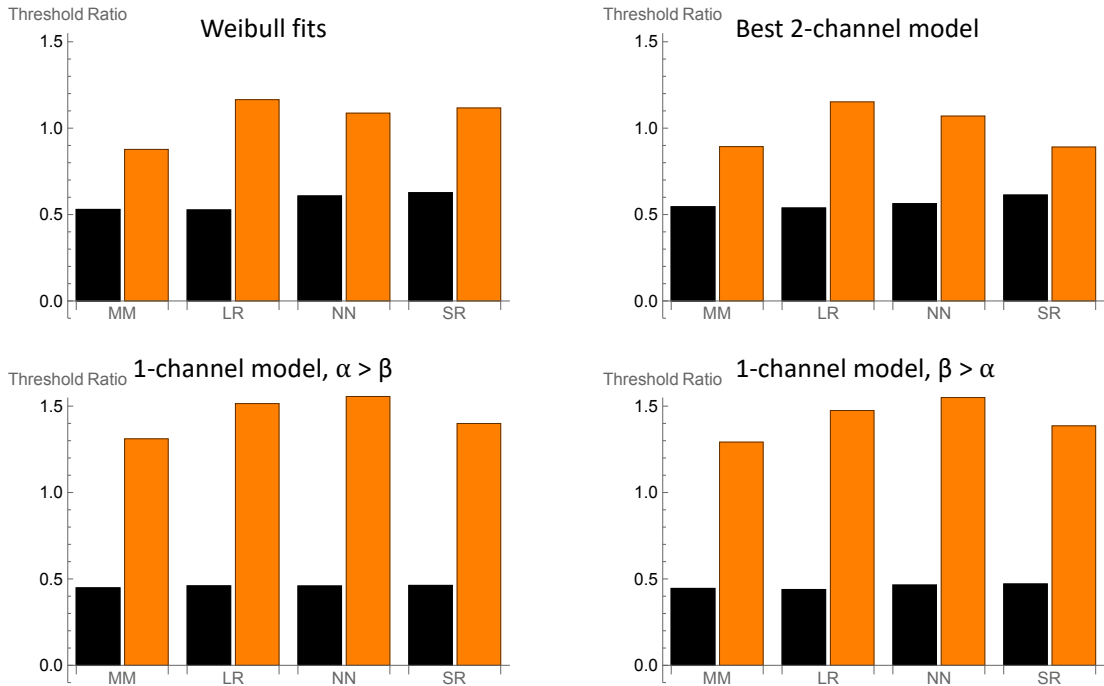
Fig. 4. Results. Threshold Ratio is the ratio between threshold (from Exp't. 2) for a compound stimulus and threshold (from Exp't. 1) for either component stimulus. Black bars represent the in-phase configuration; orange bars represent the 180° out-of-phase configuration. The 2-channel model can produce threshold ratios very similar (though not 100% identical) to those derived from Weibull fits. There is very little difference between the threshold ratios produced by the two 1-channel models. These latter ratios are very different from those derived from Weibull fits.

In Experiment 2 phase angle had a large effect on detection. This is evident from the threshold ratios. Out-of-phase thresholds were greater than In-phase thresholds, indicating that performance was better in the In-phase condition. This result implicates the existence of a channel that responds both to contrast modulations and density modulations.

To summarize the data:

(i) Performance was always better when density and contrast were in phase than when they were out of phase.

(ii) While performance in the out-of-phase condition is always worse than for the in-phase, observers could still clearly do the task.

Signal-Detection Model

In this section we describe 1-channel and 2-channel psychophysical models for detecting modulations along any arbitrary stimulus dimensions A and B. In this paper A is contrast and B is density. Similar models appeared in a recent paper by Solomon and Morgan (2020), where A and B were blur and contrast. We are indebted to a referee for alerting us to a pre-existing signal-detection model for detecting and discriminating between modulations in arbitrary stimulus dimensions (Klein, 1985). Although a full comparison between Klein's model and our own is beyond the scope of the current manuscript, one potentially critical difference is noted below.

The 1-channel model

First, consider a sinusoidal modulation along dimension A. Its amplitude and phase are a and θ_A, respectively. A general formula for the expected output of a linear mechanism is $a\alpha \cos(\theta_A - \theta_0)$, where α is the mechanism's sensitivity (or "gain") and θ_0 is its preferred phase.

Phase-independence (and square-law transduction) can be achieved using a non-linear transformation of the output from a quadrature pair of linear mechanisms:

$$\left[a\alpha \cos\left(\theta_A - \theta_0\right) \right]^2 + \left[a\alpha \cos\left(\theta_A - \theta_0 - \frac{\pi}{2}\right) \right]^2$$
$$= a^2\alpha^2 \left[\cos^2\left(\theta_0 - \theta_A\right) + \sin^2\left(\theta_0 - \theta_A\right) \right] \quad . \tag{4}$$
$$= a^2\alpha^2$$

Arbitrary power-law transduction can be achieved without sacrificing phase-independence by raising this expression to an arbitrary power $p/2$.

Now consider two sinusoidal modulations, one along dimension A and one along dimension B. Amplitudes and phases are a and b and θ_A and θ_B, respectively. A general formula for the expected output of a linear mechanism is $a\alpha \cos\left(\theta_A - \theta_0\right) + b\beta \cos\left(\theta_B - \theta_0\right)$ where α and β are the mechanism's sensitivities and θ_0 is its preferred phase. Again, phase independence (and square-law transduction) with respect to θ_0 can be achieved using a quadrature pair:

$$\left[a\alpha \cos\left(\theta_A - \theta_0\right) + b\beta \cos\left(\theta_B - \theta_0\right) \right]^2$$
$$+ \left[a\alpha \sin\left(\theta_A - \theta_0\right) + b\beta \sin\left(\theta_B - \theta_0\right) \right]^2 \quad , \tag{5}$$
$$= a^2\alpha^2 + b^2\beta^2 + 2a\alpha b\beta \cos\Delta\theta$$

where $\Delta\theta = \theta_A - \theta_B$. This too can be raised to the arbitrary power $p/2$, if necessary.

When discriminating between modulations having orthogonal orientations in space, we assume that the mechanisms are orientation selective: quadrature pairs come in opponent pairs. One opponent pair responds to positively rotated textures, the other responds to negatively rotated textures. The difference between their outputs (here symbolized by the random variable X) can be used as the basis for the observer's response.[2] Putting it all together, we can write

$$\mu_X = \pm(a^2\alpha^2 + b^2\beta^2 + 2a\alpha b\beta \cos\Delta\theta)^{\frac{p}{2}} \tag{6}$$

---

[2] Klein (1985) makes no analogous assumption. In this sense, his model may be more general than ours.

for the expected output from a quadrature pair, given two sinusoidal inputs with amplitudes a and b and phase angle $\Delta\theta$. Without loss of generality, we may assume that the variance is $\sigma^2 = 1$. The observer should decide the stimulus has negative (anti-clockwise) tilt if and only if output exceeds some arbitrary criterion b_θ. The observer would be unbiased only if $b_\theta = 0$.

The 2-channel model

As foreshadowed by the green and orange bars in Fig. 4, the 1-channel model cannot produce a quantitatively satisfying fit to our data. Consequently, in this subsection, we extend the model to two channels. The 2-channel model can produce a quantitatively satisfying fit.

Whereas output from the first channel was modelled using the Normal random variable X, output from the second channel is modelled using the Normal random variable Y, with expectation $\mu_Y = \pm(a^2\alpha'^2 + b^2\beta'^2 + 2a\alpha'b\beta' \cos\Delta\theta)^{\frac{p'}{2}}$ and variance $\sigma_Y^2 = 1$. The second channel is identical to the first, except for different gains (α' and β') and a possibly different power-function transducer ($p'/2$). At this stage, we diverge from the model discussed by Solomon and Morgan (2020) and assume $\text{cov}(X, Y) = 0$ for computational convenience.

Imagine the plane of all possible outputs from two mechanisms (see Fig. 5 for an illustration). Given this (2-D) space of channel outputs, a (1-D) linear discriminant is the simplest decision rule we could imagine: $y = m_\theta x + b_D$. The model observer decides that the stimulus has positive (clockwise) tilt if and only if the point representing the two channels' outputs lies above the line. The probability of a positive response is given by

$$p_1 = \int_{-\infty}^{\infty} \int_{-\infty}^{\infty} H(y - m_\theta x - b_\theta)\, f(x,y)\, dxdy, \qquad (7)$$

where H is the Heaviside step function and f is the bi-variate normal density with mean and variance

$$\mu = \begin{bmatrix} \mu_X \\ \mu_Y \end{bmatrix}, \Sigma = \begin{bmatrix} 1 & 0 \\ 0 & 1 \end{bmatrix}; \qquad (8)$$

the probability of a negative response is given by $1 - p_1$. For ease in computation, model fits are obtained with a simplified, equivalent form of Equations 7 and 8:

$$p_1 = \frac{1}{2}\,\mathrm{erfc}\left(\frac{b_\theta + m_\theta \mu_X - \mu_Y}{\sqrt{2}\sqrt{1+m_\theta^2}}\right), \tag{9}$$

where erfc is the complementary error function.

Fig. 5 contains a graphical interpretation of the model's fit to a representative observer's data from Experiment 2. The relevant parameter values have been highlighted with yellow in Table 2. Thus, X channel has gains $\alpha = 4.26$ and $\beta = 2.61$ on the two inputs A and B and the Y channel has gains $\alpha' = 4.83$ and $\beta' = 0$. We can now interpret Fig. 5 as follows. The X channel has inputs from both signals (density and contrast) and thus, in the case where the signals are in-phase, has a greater output than the Y channel, which receives input from only the contrast signal. When the inputs are $180°$ out of phase, they partially cancel in the X channel but not in the Y channel. Consequently, the Y channel has a larger output than the X channel.
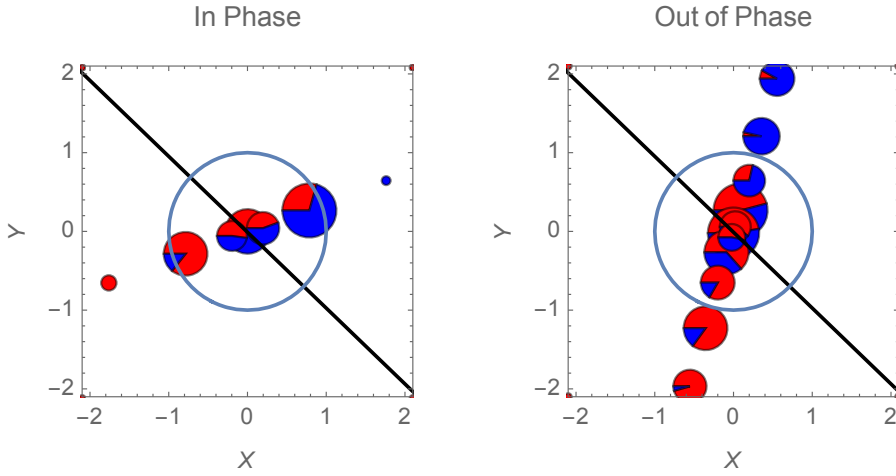

Fig. 5. Graphical interpretation of the 2-channel model's fit to a representative observer's data from Experiment 2. Each pie chart represents one combination of stimulus orientation ($\pm 45°$, with respect to vertical), phase angle (in phase, or out-of-phase), and modulation amplitude. Larger pie charts indicate more trials. Red and blue sectors illustrate the frequencies with which observer MM reported that the tilt was positive and negative, respectively. The horizontal position of each pie chart shows the first channel's expected output (signed so that positive values are associated with positive tilt), and the vertical position shows the second channel's expected output. Inputs are not represented in the diagram. Also not shown are Gaussian blobs centred on each one of these pie charts. Each blob describes the density of the joint likelihood for the two channels' responses. That likelihood has unitary standard deviation in each dimension. The circle describes one standard deviation in every direction around the origin. The black line serves as the

discriminant: stimuli that produce responses to its left and right are classified as having negative and positive tilts, respectively.

Model fits

As described below, we placed various constraints on the signal-detection model, when (simultaneously) fitting it to the data from Experiments 1 and 2. In all cases, we allowed for the possibility of a non-zero lapse rate, i.e., a proportion of trials on which the observer selects a response at random (regardless of the stimulus). In all cases, maximum-likelihood fits were obtained when the lapse rate was zero.

As mentioned above, the results of Experiment 2 strongly implicate the existence of a channel that responds both to contrast modulations and density modulations. To see whether a single-channel model would prove sufficient to explain these results, we obtained maximum-likelihood fits of the 1-channel (4-parameter) model. Specifically, we used Mathematica's implementation of Brent's (2002) principal-axis method to find maxima (with 3 digits of accuracy) in the function mapping parameter values to log likelihood. When fitting the 1-channel model, this function had two distinct peaks: one with relatively greater gain for contrast modulations, the other with greater gain for density modulations. Had we separately manipulated the modulation amplitudes of contrast and density, we might have been able to determine which of these two components of our stimulus had a greater effect on performance. However, we didn't. The twin peaks in our energy functions arise because the ratio of modulations depths ($m_\mathrm{d}/m_\mathrm{c}$) was held constant throughout the experiment.

When fitting the 2-channel model, we found that good fits could be obtained when any one of the four gains (α, β, α', or β') was fixed at zero. Table 2 contains parameter values for maximum likelihood when fixing $\beta = 0$. It also contains parameter values for maximum likelihood when fixing $\alpha' = 0$.

The 2-channel model produces a significantly better fit to the data, compared to the 1-channel model, because the latter necessarily over-estimates the effect of phase angle in Experiment 2, while struggling to maintain the baseline thresholds from Experiment 1: either the model's threshold for contrast modulation is too low and its

threshold for density modulation is too high or vice versa (see Supplementary Fig. S2). In summary, the best-fitting 2-channel model for all observers contains one channel that is sensitive to both density and contrast; and a second channel that is sensitive to only one of these dimensions. The model cannot distinguish whether this single dimension is contrast or density.

DISCUSSION

It is important to be clear at the outset that our model is not intended to represent specific anatomical structures in the human visual system. Instead, we have described computations that are sufficient for producing results like those of our human observers. Nonetheless, we can be fairly confident that there must be at least one physiological mechanism that is sensitive to both contrast and density modulations over space. The existence of this mechanism is implied by the effect of phase angle when contrast and density modulations are combined. In this respect, our experiments confirm and extend the findings Mulligan and MacLeod (1988) obtained with luminance-modulated dot textures. They invoke a mechanism that carries out areal summation of a signal from mechanisms sensitive to luminance. Similarly, we invoke areal summation of a signal related to contrast energy, for example, from retinal ganglion cells or cortical cells with rectifying contrast-sensitive subunits (e.g., Hochstein and Shapley (1976)). Such a mechanism would inevitably confound changes in contrast and changes in density/numerosity. Our mechanism may be related to the contrast integrator described by Meese & Summers (2007) and Baker & Meese (2016), although they measured contrast thresholds for sparsely scattered texture elements themselves, while we measured orientation-discrimination thresholds for contrast/density modulations.

Although the out-of-phase condition was clearly more difficult (i.e., thresholds were higher) than the in-phase condition, it was not impossible. This fact suggests that observers had more than one mechanism (with non-zero gain for contrast and/or density modulations) at their disposal. Indeed, within the framework of signal-detection theory, a simple 1-channel model proved incapable of producing sufficiently low thresholds in Experiment 2's out-of-

phase condition without simultaneously over-elevating one of the detection thresholds (i.e., for either contrast or density modulations) from Experiment 1.

Although the out-of-phase condition was not impossible, the mechanism responsible for that task may have been very different from the opponent quadrature pairs of our signal-detection model. Contrast energy might have been uniform across our out-of-phase stimuli, but we know that higher-order modulations of texture, invisible to an energy mechanism, are detectable by human observers given sufficient time for inspection (e.g., Julesz, 1971, Nothdurft, 2007).

The perceptual impressions created by textures are not traceable to subjectively precise localization and characterization of the texture elements. Such impressions may depend on the statistics of neural activation patterns rather than on the individual peaks and troughs of activation profiles evoked by each example of a texture class. In the present experiments, not only the mean activation but the histogram of activations may be diagnostic. If the neurons of a contrast energy channel have receptive fields that span only a few texture dots, they will respond more uniformly in a low-contrast, high-density region than in a low-density, high-contrast region. This could potentially allow the observer to perform the task of our Experiment 2, when the mean activation of the contrast energy channel is the same in these two cases, thereby salvaging the single channel model in a more complex form where the histogram of contrast energy may be diagnostic (Chubb, Econopouly, & Landy, 1994).

In conclusion, we can be confident that there is at least one channel in which density and contrast are combined into a single mechanism. Furthermore, there must in addition be a texture mechanism for detecting out-of-phase modulations in density and contrast, which may or may not be another kind of energy mechanism.

| Observer	Experiment 1					Experiment 2				
	Contrast		Density		ln L	In-phase		180° Out-of-phase		ln L
	λ	k	λ	k		λ	k	λ	k	
MM	0.263	2.50	0.204	2.87	−454.440	0.529	4.67	0.877	2.62	−327.724
LR	0.120	2.63	0.084	1.96	−328.425	0.527	1.72	1.165	1.66	−553.517
NN	0.120	1.75	0.119	2.00	−345.121	0.608	2.26	1.087	2.66	−372.876
SR	0.138	1.64	0.143	2.77	−402.690	0.627	2.33	1.117	3.03	−413.165

Table 1. Summary of psychometric data by the maximum likelihood (L) Weibull Functions (Eqn. 3) of single component (contrast or density) modulation amplitude (Experiment 1) and a common multiple of the single-component detection thresholds (Experiment 2).

Observer	α	β	p	α'	β'	p'	m_θ	b_θ	$\ln L$
MM	6.49	3.92	1.16	0	0	1	−1	−0.01	−827.9
	3.13	7.90	1.30	0	0	1	−1	0.01	−824.9
LR	15.0	11.4	1.10	0	0	1	−1	0.32	−887.5
	8.80	22.9	0.96	0	0	1	−1	0.31	−887.3
NN	13.6	7.64	1.01	0	0	1	−1	0.13	−740.5
	7.17	13.9	1.03	0	0	1	−1	0.14	−740.1
SR	12.1	6.35	1.02	0	0	1	−1	−0.32	−843.5
	6.05	12.6	1.06	0	0	1	−1	−0.35	−841.6
MM	3.93	0	1.82	1.85	5.33	2.34	−0.97	−0.01	−782.6
	4.26	2.61	1.98	0	4.83	2.19	−0.97	−0.01	−782.6
LR	6.54	0	1.63	6.22	14.4	1.38	−1.02	0.33	−861.2
	10.7	8.48	1.71	0	8.47	1.71	−0.71	0.28	−860.6
NN	5.96	0	2.12	5.50	10.7	1.39	−1.31	0.16	−715.9
	11.8	6.48	1.36	0	5.94	2.09	−0.60	0.11	−715.8
SR	7.24	0	1.65	2.22	7.83	2.09	−1.05	−0.35	−796.3
	7.63	2.79	1.43	0	7.27	2.45	−1.31	−0.40	−794.7

Table 2. Parameter values maximizing the likelihood of 1-Channel (Rows 1-4) and 2-Channel (Rows 5-8) model fits to the psychometric functions.
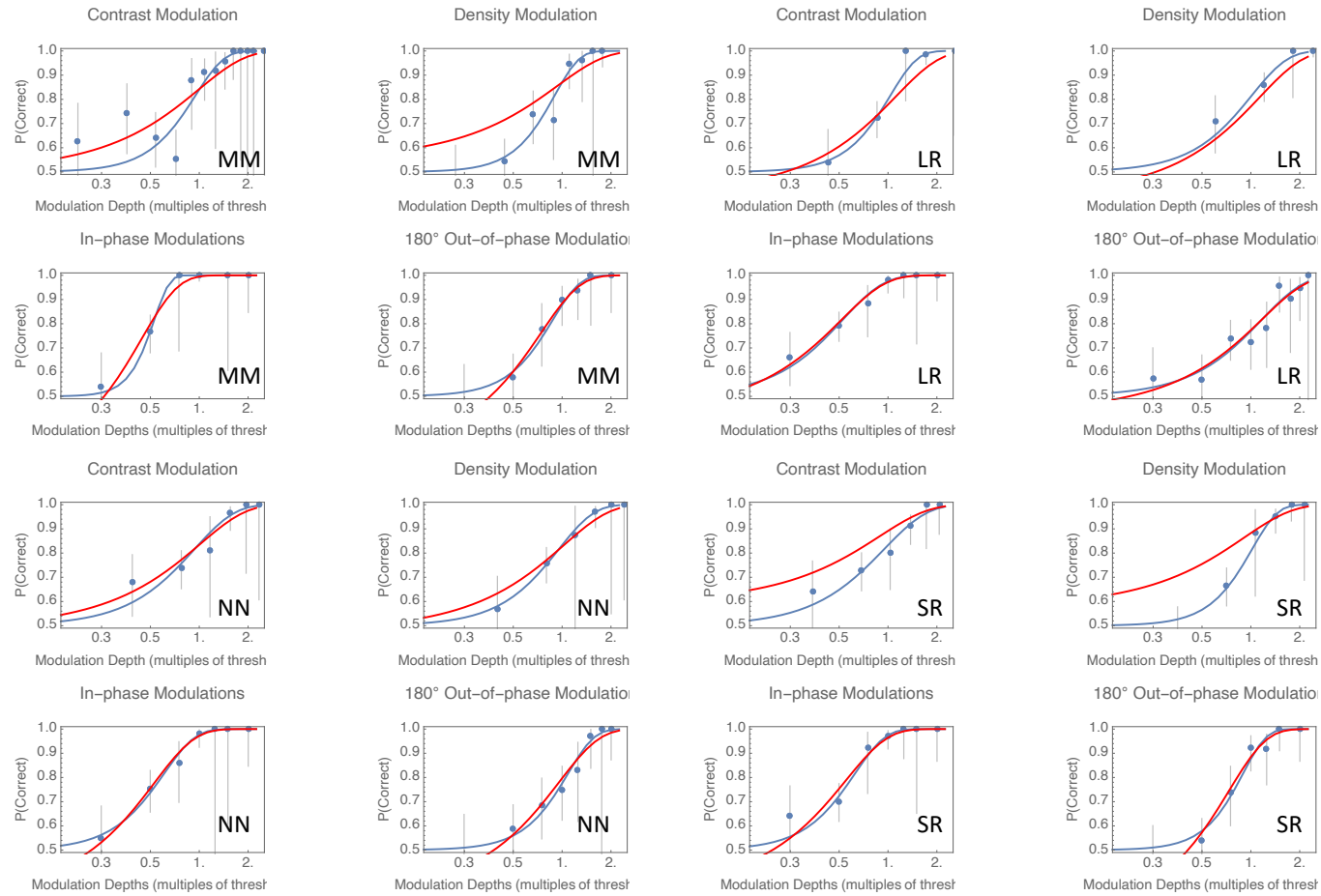
Supplementary Fig. S1. A comparison between Weibull and Gaussian psychometric fits. Each point shows the frequency of correct responses, for a given multiple (excluding zero) of detection threshold. Experiment 1 is illustrated in rows 1 and 3; Experiment 2 in rows 2 and 4. Blue and red curves illustrate (atheoretical) Weibull and Gaussian summaries, respectively. Error bars contain 95% Binomial confidence intervals.
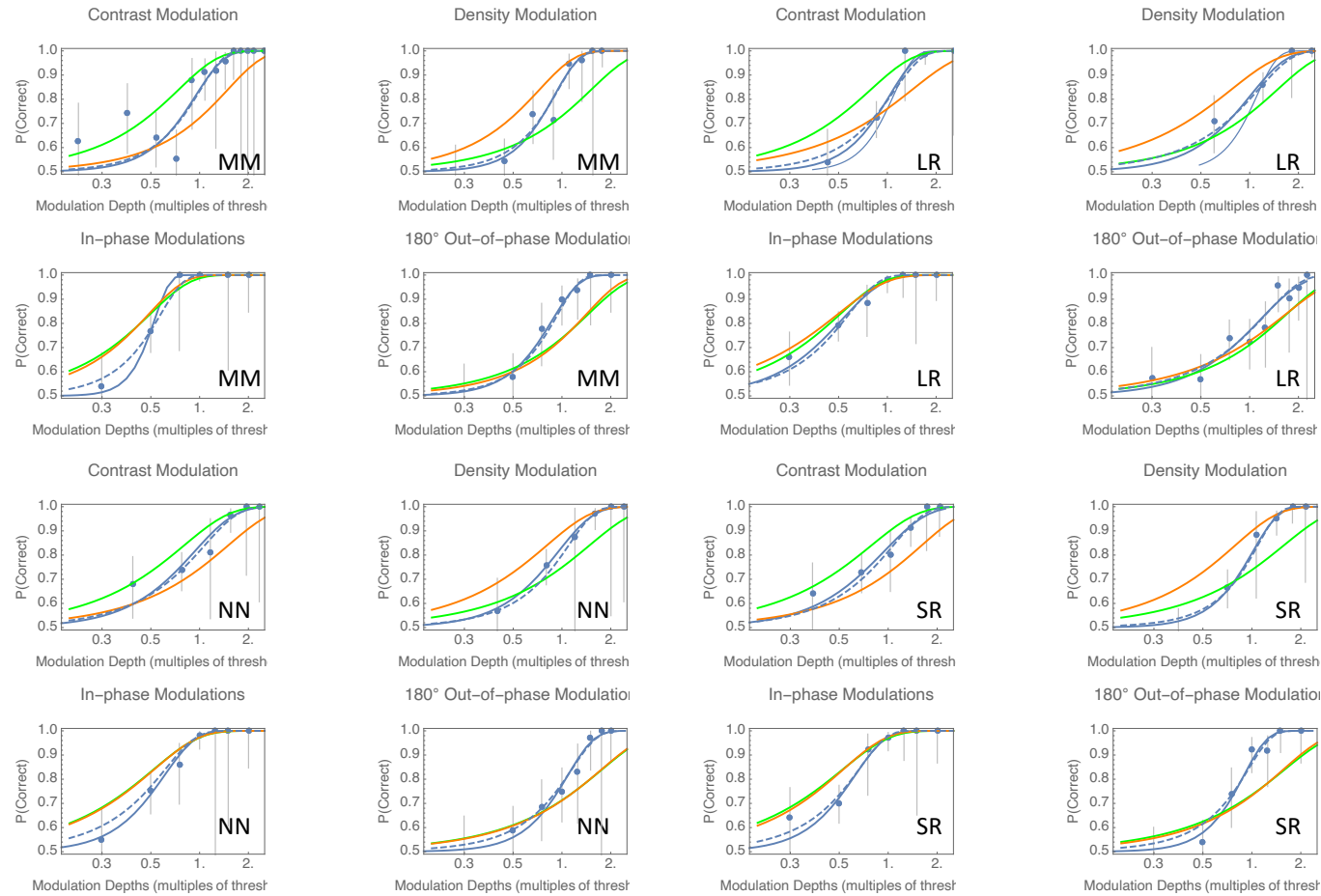
Supplementary Fig. S2. All results with model fits. Each point shows the frequency of correct responses, for a given multiple (excluding zero) of detection threshold. Data from each observer are illustrated. Predictions of two models are illustrated by the smooth curves. Solid blue curves illustrate atheoretical (Weibull) summaries with 8 free parameters (two per panel) per observer. Dashed blue curves illustrate the best fit of a two-channel, 7-parameter (per observer) signal-detection model. Orange and green curves illustrate the best fits of a one-channel, 4-parameter

version of the signal-detection model, in which contrast gain is constrained to be greater than density gain and vice versa, respectively. Error bars contain 95% binomial confidence intervals.

REFERENCES

Baker, D.H. & Meese, T.S. (2016) Grid-texture mechanisms in human vision: Contrast detection in regular sparse micro patterns requires specialist templates. Scientific Reports, 6, Article Number: 29764, doi:10.1038/srep29764

Brent, R. P. Algorithms for Minimization without Derivatives. Dover, 2002 (Original edition 1973).

Chubb, C., Econopouly, J. & Landy, M.S. (1994) Histogram Contrast Analysis and the visual segregation of IID textures. *Journal of the Optical Society of America A*, 9, 2350-2374.

Hochstein, S. & Shapley, R.M. (1976) Linear and nonlinear spatial subunits in Y cat retinal ganglion cells. J. Phyisiol., 262(2),65-84.

Meese, T. S. & Summers, R. J. (2007) Area summation in human vision at and above detection threshold. *Proc R Soc. B* **274**, 2891–2900.

Julesz, B. (1971). *Foundations of Cylopean Perception*. Chicago: University Press.

Klein, S. A. (1985) Double-judgment psychophysics: problems and solutions, *J. Opt. Soc. Am. A 2*(9) 1560–1585.

Kleiner, M., Brainard, D., Pelli, D., (2007) What's new in Psychtoolbox-3? Perception. 36 ECVP Abstract Supplement 14.

Mood, A., Graybill, F. & Boes, D. (1974). Introduction to the theory of statistics, 3rd edn. New York, NY: McGraw-Hill.

Morgan, M. J., Raphael, S., Tibber, M. S. & Dakin, S. C. (2014) A texture processing model of the 'visual sense of number'. Proc. Roy. Soc.

B., 281, 20141137.

Mulligan, J.B. & MacLeod, D.I.A (1988) Reciprocity between luminance and dot density in the perception of brightness. Res., 28, Vision Res., 503-519.

Nothdurft, H-C. (2000) Salience from feature contrast: additivity across dimensions. Vision Res., *40*, 1183-1201.

Raphael S, Morgan M.J (2016) The computation of relative numerosity, size and density. Vision Res 124: 15-23

Saarela, T.P. & Landy. M.S. (2013) Combination of Texture and Colour cues in visual segmentation. Vision Res., 58. 59-76.

Solomon, J. A. & Tyler, C. W. (2018) A Brücke-Bartley effect for contrast. *Royal Society Open Science, 5*: 180171.

Solomon, J. A. & Morgan, M. J. (2020) Models for discriminating image blur from loss of contrast. *Journal of Vision*, 20(6):19, 1–14.

Watson, A. B. (1979). Model of visual contrast gain control and pattern masking. Vision Res. 19 (5), 515-522.

Watson, AB & Ahumada, AJ (2011) Blur clarified: A review and synthesis of blur discrimination Journal of Vision, 11(5):10, 1–23
Watt, R. J. & Andrews, D. (1981) APE: Adaptive probit estimation of psychometric functions. Current Psychological Reviews 1(2), 205-213.